International Journal of Hydrogen Energy 94 (2024) 1374–1388

Contents lists available at ScienceDirect

International Journal of Hydrogen Energy

journal homepage: www.elsevier.com/locate/he

Passive autocatalytic recombination of hydrogen on a Pt/Al_2O_3-coated metal foam: Experimental evaluation and CFD modelling

Kyatsinge Cédric Musavuli [a], Alexander Malakhov [a], Raymond Cecil Everson [b], Alina Kozhukhova [a], Phillimon Modisha [a], Dmitri Bessarabov [a,*]

[a] HySA Infrastructure Centre of Competence, Faculty of Engineering, North-West University, Private Bag X6001, Potchefstroom, 2531, South Africa
[b] Centre of Excellence in Carbon-based Fuels, School of Chemical and Minerals Engineering, Faculty of Engineering, North-West University, Private Bag X6001, Potchefstroom, 2531, South Africa

ARTICLE INFO

Handling Editor: Ramazan Solmaz

Keywords:
Hydrogen safety
Passive autocatalytic recombination
Metal foam
Pt catalyst
CFD modelling
Experimental validation

ABSTRACT

Pt/Al_2O_3-coated Al foams were tested for the passive autocatalytic recombination of H_2. The characterisation of the washcoat surface confirmed the uniform distribution of Pt and Al_2O_3 over the entire washcoat surface. Transmission electron microscopy results revealed a slight increase in particle size from 3.8 to 6.2 nm after prolonged reaction. High H_2 conversions of 57–89% are achieved and the catalyst activity is maintained for >480 h on stream. The performance of the foam-based catalyst bed is similar to that of plates but surpasses that of catalyst pellets. Temperatures recorded at the hottest spots on the foam surface reach a maximum of only 393 °C at the highest H_2 inflow. Computational fluid dynamics simulations were performed on the actual foam geometry obtained using computed tomography. The simulations demonstrate the importance of thermal radiation in the model. There is good agreement between results of experimental H_2 conversions and maximum combustion temperatures.

1. Introduction

In order to limit the global temperature rise to <1.5 °C by 2050, the industrial sector is slowly shifting from fossil fuel to low- or zero-carbon energy sources, such as hydroelectricity, tidal, geothermal, solar and wind energy. Due to the irregular distribution and intermittent nature of several of these sources, causing an imbalance between energy supply and demand, several energy storage technologies are currently being developed. They include flywheels, superconductors, supercapacitors, batteries, compressed air, pumped hydro, phase change materials (latent heat) and chemical storage [1–4]. The chemical storage technique is considered as one of the most realistic options for long-term storage of relatively large amount of energy. This method consists using excess renewable power to produce a chemical compound, known as energy carrier [5]. Green H_2, produced by water electrolysis, has been proposed as a suitable energy carrier due to its high gravimetric energy density (120 MJ/kg), the relative maturity of its production and utilisation technologies [6]. It is also a highly versatile gas; it can be used for energy production in fuel cells or microcombustors, the reduction of metal ores, and the synthesis of industrial chemical products (ammonia, methane, methanol) and sustainable aviation fuels [7,8].

With such an increasing amount of H_2 being handled in industries of various sizes, there is a clear need for the application of strict safety measures [9]. H_2 leaks in air can pose significant risks of deflagration or detonation in an environment where the gas' self-ignition temperature of ~585 °C is reached within its flammability limits (4–75 vol% H_2 at normal temperature and pressure) [10,11]. Reported methods of H_2 removal include ventilation, deliberate ignition and passive autocatalytic recombination (PAR) [12]. For risk mitigation, ventilation is not always effective due to the high buoyancy of H_2, which can cause the gas to accumulate in dead corners and increase the formation of high-risk zones near the upper sections of confined spaces. On the other hand, deliberate ignition could cause the unintentional formation of NOx gases as combustion temperatures increase to >800 °C [13]. The advantage of PAR technology lies in its ability to prevent the accumulation of H_2. Spontaneous combustion commences at ambient temperature, at low H_2 concentrations (i.e., within the first instants of an accidental leak), without reaching temperatures favourable to the formation of NOx, and releasing only water as product (Eq. (1)) [14]. A recombiner can be installed in confined or semi-confined spaces, as well as underground

* Corresponding author.
E-mail address: dmitri.bessarabov@nwu.ac.za (D. Bessarabov).

https://doi.org/10.1016/j.ijhydene.2024.11.116
Received 13 September 2024; Received in revised form 5 November 2024; Accepted 7 November 2024
Available online 18 November 2024

parking, tunnels or mining facilities [15].

$$H_2 + \frac{1}{2}\,O_2 \rightarrow H_2O \qquad \Delta H = -241\ kJ \Big/ mol \tag{1}$$

Arguably, the most important feature of a recombiner is its catalytic section. Pd and Pt have been reported as two of the most studied PAR catalysts due to their low light-off temperatures and high catalytic activities at temperatures <500 °C [16]. However, these noble metal catalysts have a high tendency for sintering at increasing combustion temperatures, resulting in significant loss of catalytic activity. One way to prevent this problem is to use a high-surface morphological support such as alumina, ceria, yttria or zirconia [13,17]. These supports improve the dispersion of active metal nanoparticles (NPs), limit their mobility and prevent their aggregation [11,18]. Du Preez et al. [18] demonstrated the importance of the presence of a morphological support for their Pt sputter-coated on Ti meshes. They showed that the abundance of an oxide layer prevented the aggregation of Pt nanoparticles. This high-surface oxide layer improved the catalyst long-term stability.

Another preventive option is making use of high thermal conductivity materials (e.g. metals such as Al, Cu, Ti) as catalyst support structures. They efficiently distribute the heat released through chemical reaction, thus preventing the occurrence of hot spots at which local aggregation of the NPs could occur [13,14]. Further process intensification could be achieved through the use of porous materials such as open-cell metal foams, which have outstanding heat and mass transport properties [19,20]. These high-surface catalyst support structures facilitate not only mass transport through radial reactant mixing and increased tortuosity, but also heat transport by convection and conduction [21,22].

Experimental studies on catalytic H_2 combustion on foams are reported in literature. A study by Jo et al. [20] offers clear insight into the effects of the inlet H_2 feed rate, the active metal (Pt) content and morphological support (Al_2O_3) loadings on H_2 conversions, and the maximum temperatures obtained during the H_2 combustion process in a tubular reactor. Jin and Kwon [23] investigated the performances of a Pt/Al_2O_3-coated Ni foam and Pt-coated ceramic foam for H_2 combustion at different feed gas flow rates and equivalent ratios ($0.5H_2/O_2$ molar ratio). They reported the effects of these operating parameters on the H_2 conversion rates and the maximum temperatures achieved. Furthermore, they discussed the potential effects of the water vapour generated during the process. Fumey et al. [24] developed a H_2-based cooker for domestic applications utilising uncoated and Pt-coated SiC foams as gas diffuser and catalyst bed, respectively, for the combustion of H_2. They reported the effects of the H_2 flow and equivalence ratios on the water heating efficiency of the device. Fernandez et al. [25] conducted H_2 combustion experiments on a clay-bound SiC foam coated with Pt/Al_2O_3–CeO_2. This foam-based catalytic system exhibited a high catalytic performance even at lean H_2/air mixtures and at ambient conditions. Their findings demonstrated the suitability of foam-supported catalysts for H_2 combustion processes.

To further understand the benefits of conducting H_2 combustion processes in foam-based catalytic reactors, particularly in the context of accidental H_2 release, it is considered important to study the difference between different catalyst bed structures. Furthermore, it is important to investigate the effects of prolonged exposure of the catalyst to the reaction medium in order to assess the catalyst durability or resistance to deactivation by sintering [13,14,26].

The PAR process has also been investigated through simulations based on theoretical and analytical knowledge of fluid dynamics and chemical reactions. Computational fluid dynamics (CFD) tools such as Ansys Fluent, COMSOL Multiphysics, STAR-CCM + or OpenFOAM have been used to simulate the complex chemistry and transport behaviour of the reacting gas in different processes. The focus of the reported H_2 combustion simulations has usually been on the estimation of temperature, velocity, or gas composition profiles in relatively simple geometries [15,27–33]. For instance, Zanoni et al. [15] developed a CFD model, using COMSOL Multiphysics, to simulate the PAR process on rectangular stainless steel plates. They investigated the effects of inlet flow conditions (H_2 concentration, gas velocity) and plate spacing on the temperature profile along the plate height, the H_2 and CO recombination rates, the surface reaction and the catalyst poisoning by CO. Malakhov et al. [10] used STAR-CCM + for the CFD simulation of the PAR process in a recombiner consisting of cylindrical ceramic rods. Temperature profiles and H_2 recombination efficiencies were assessed at different H_2 inlet mole fractions. Experimental results were used for model validation. Kim et al. [33] conducted transient CFD simulations in OpenFOAM to study the PAR of H_2 under oxygen (O_2)-rich and O_2-lean conditions in industrial plate-based recombiners. Their study compared a correlation-based model with a mass-diffusion model and results demonstrated the importance of O_2 diffusion on the H_2 recombination, especially under O_2-lean conditions.

To simulate more complex fluid behaviours occurring in irregular geometries, an accurate 3D rendering of the solid domain (foam) can be obtained using computed tomography (CT). Here, inaccuracies of the simulation will be only due to the uncertainties related to the differential equations, assumptions and boundary conditions chosen to describe the model [34].

In the present study, a 5 wt% Pt/Al_2O_3 catalyst coated on Al foams was tested in a PAR reactor set-up, previously reported by Malakhov et al. [10]. There is currently a need for comparison between different catalyst configurations containing the same amount of Pt/Al_2O_3 catalyst. Besides, there is no known fully heterogeneous 3D CFD simulation of PAR processes conducted on foam-supported catalysts. The objectives of our study are the following: (1) Characterise Pt/Al_2O_3-coated foams and evaluate their catalytic performance in a passive autocatalytic recombiner using steady-state H_2 conversions and coated foam surface temperatures as the main performance criteria. (2) Compare the performance of a recombiner using a Pt/Al_2O_3-coated foam, Pt/Al_2O_3-coated plates or Pt/Al_2O_3 pellets in its catalytic section. (3) Carry out a durability test of the foam-supported Pt/Al_2O_3 catalyst. (4) Carry out a fully heterogeneous CFD modelling of the catalytic H_2 combustion process using accurate 3D geometry of the foam samples in the PAR reactor set-up. The experimental section of this study will give an insight into the difference in performances between geometric configurations of the catalyst bed in the same recombiner. The numerical modelling will provide a deeper understanding of the flow phenomena and temperature profiles inside a foam-based recombiner.

2. Materials and methods

2.1. Catalyst preparation and coating procedure

The 5 wt% Pt/Al_2O_3 catalyst was prepared in-house by the wet impregnation method: 150 g γ-alumina pellets (Sasol, South Africa) were soaked, at ambient temperature, in an aqueous solution containing 19.2 g 38 wt% hexachloroplatinic acid (H_2PtCl_6) (HySA Infrastructure, South Africa). The water was then removed by evaporation at 60 °C and a pressure of 46 mbar in a Büchi Rotavapor® R300 (BÜCHI Labortechnik AG, Switzerland), equipped with an evaporating flask, rotating at a speed of 40 rpm. The H_2PtCl_6-impregnated alumina was subsequently dried in an EcoTherm oven (Labotec, South Africa) at 120 °C for ~4 h. Calcination and reduction of the dried pellets was performed at 350 °C (ramp rate 10 °C/min) over a period of 2 h in a stream of air and 50 vol% H_2/N_2 (flow rate 250 mL/min), respectively, using a CTF12 horizontal tube furnace (Carbolite Gero, England).

Aluminium foams (Recemat BV, Netherlands) of pore density 10 PPI (pores per inch) and 95% porosity were cut into four blocks (70 mm × 40 mm × 10 mm) and cleaned in 99.5 vol% ethanol (Rochelle Chemicals, South Africa) for 10 min to remove any organic impurities from the substrate surface. Pt/Al_2O_3 pellets sampled from a batch prepared using

the method described above were crushed into fine powder and later used for preparation of the slurry. This slurry consisted of ~30 wt% of the Pt/Al_2O_3 powder in an aqueous solution containing 1.5 wt% polyvinyl alcohol (MCL, South Africa) as binder, and 0.1 M HCl as dispersant and etching agent to increase the roughness of the aluminium foam surface [22,35,36]. The mixture was thoroughly homogenised (400 rpm, 60 °C, 1 h) using an AccuPlate hotplate stirrer (Labnet International, NJ, USA). The clean and dry foams were then dipped into the slurry. A constant flow of compressed air was used to remove the excess slurry blocking the foam pores. The foam samples were subsequently dried and the process was repeated until the desired amount of catalyst was coated on the foam struts. To stabilise the washcoat layer, the dry coated foams were calcined in air and reduced in 50 vol% H_2/N_2 (flow rate 250 mL/min) at 350 °C in the tube furnace. The same procedure was used to coat the four aluminium plates (70 mm × 40 mm × 2 mm). These were first scraped with sandpaper to increase their surface rugosity and improve the adhesion of the catalyst. The foam and the plate samples were coated with 3.8 g Pt/Al_2O_3 and their performances compared with that of the same amount of Pt/Al_2O_3 pellets.

2.2. Characterisation

The surface morphologies of the Pt/Al_2O_3-coated foams, Pt/Al_2O_3-coated plates and Pt/Al_2O_3 pellets were characterised using a FEI Quanta FEG 250 field emission gun scanning electron microscope (Thermo Fisher Scientific, USA). Elemental mapping of the washcoat surface was performed with energy dispersive X-ray spectroscopy (EDS) using an X-Max SDD 20 mm^2 detector (Oxford Instruments, England). Scanning electron microscopy (SEM) micrographs were analysed using xT Microscope Server and xT Microscope Control software, while EDS data were processed using AZtec software. Pt NPs were observed via transmission electron microscopy (TEM) using an electron microscope (JEOL JEM 2100, Japan) at 200 kV. Samples were dissolved in ethanol and sonicated for about 30 min then dispersed on a carbon-coated copper grid for analysis. Mean particles sizes were calculated from at least 150 particles obtained from TEM images using the open-source ImageJ program. TEM was performed before and after the long-term utilisation of the Pt/Al_2O_3-coated foam in the PAR process in order to gain insight into the effect of prolonged utilisation on the Pt NPs.

Characteristic dimensions of the coated and uncoated foam samples were determined by CT using the Nikon XT 225 system (Nikon Corporation, Tokyo, Japan) of the Central Analytical Facilities of Stellenbosch University, South Africa [37]. In this process, a voxel size of 55.85 µm was utilised and X-rays were generated at 100 kV and 500 µA. Captured images were analysed with the system-supplied Datos reconstruction software for the reconstruction of the volumetric dataset and the generation of the stereolithography (STL) file. VGSTUDIO MAX 2024.1 (Volume Graphics, Heidelberg, Germany) was used for the visualisation and quantitative analysis of the generated 3D geometry (STL file). From the CT-generated database, the gravimetric surface area, pore density, and the pore and strut diameters of the foam samples were calculated.

2.3. Experimental evaluation

Fig. 1 shows the two different set-ups in which catalytic H_2 recombination experiments were conducted: first, a recombiner [10], for performance evaluation of the Pt/Al_2O_3-coated foams and further comparison with two catalyst structural configurations previously reported in the literature (plates and pellets) [14,26,38] and, second, a tubular fixed-bed reactor for durability tests on the foam-supported Pt/Al_2O_3 catalyst [26,39].

2.3.1. PAR experiments

PAR experiments were conducted in a rectangular recombiner (280 mm × 242 mm × 45.5 mm) that contained the four Pt/Al_2O_3-coated foams (Fig. 1a). At the recombiner inlet, 99.9 vol% H_2 (Hydrogen South Africa Infrastructure, South Africa) and compressed air flow were adjusted using thermal mass flow controllers (EL-FLOW F-201AV, Netherlands). The gas mixtures were then feed to the recombiner inlet (lower section) through a pipe (diameter 10 mm) that distributed premixed mixtures of H_2 and air through 12 holes (diameter 0.5 mm). The mixture was passed through a perforated plate to prevent uneven distribution of the gas as at the catalyst region (middle section) where the recombination occurred. The product gas mixture (H_2, O_2, N_2, H_2O) exited the recombiner through its outlet (top section) and was vented to the atmosphere. Three XEN-5320 H_2 sensors (Xensor Integration, Netherlands) were fitted at the recombiner inlet section and three more at the outlet section. The sensor data were recorded every second and then used for calculation of the H_2 conversions at the different flow

Table 1
Operating parameters used during the catalytic activity test in a PAR set-up.

Parameters	Values
H_2 inlet concentration (vol%)	2–6 (increments of 1%)
Gas injection velocity (m/s)	2.0, 5.0, 7.5 and 10

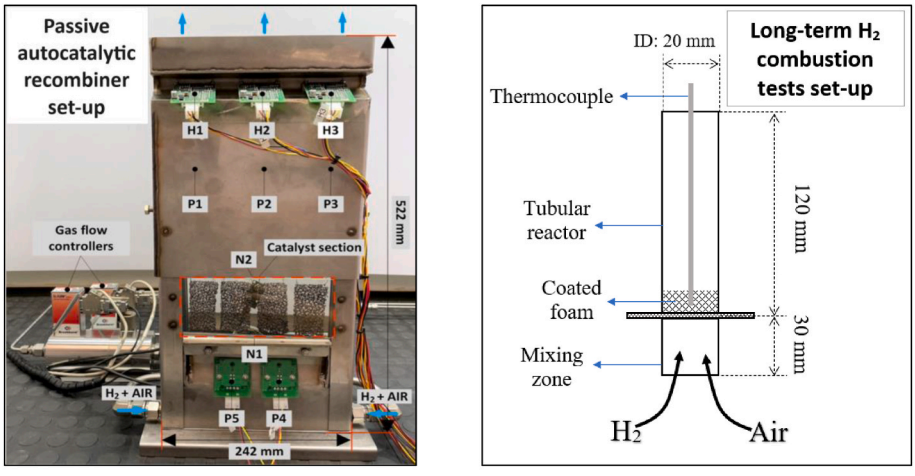

(a) (b)

Fig. 1. (a) Image of the reactor set-up used in the PAR experiments. (b) Schematics of the tubular reactor used for the durability tests. (Legend. H1–H3 and P1–P5: H_2 sensors).

conditions as given in Table 1.

Performance assessment was based on the steady-state H_2 conversions and average temperatures recorded on the foam surface at different operating conditions. H_2 conversions were evaluated using Eq. (2), in which the number of moles n_{H2in} was calculated from the gas flow rate, and the inlet and outlet H_2 concentrations. Selected experiments were conducted in triplicate to ensure the repeatability of results. The average deviation in H_2 conversions was ~5%.

$$X_{H2} = \frac{n_{H2in} - n_{H2out}}{n_{H2in}} \quad (2)$$

Surface temperatures were recorded every second using Reveal IR software (Telops, Canada), while temperature profiles were analysed using a high-resolution M100hd IR camera (Telops, Canada) equipped with lenses capable of detecting electromagnetic intensities corresponding to temperatures in the range 0–2500 °C.

2.3.2. Durability tests

The durability of a foam-supported Pt/Al_2O_3 catalyst was tested in a tubular reactor in which a 10 PPI foam disk (diameter 20 mm, height 10 mm) coated with 0.2 g Pt/Al_2O_3 was placed 3 mm above the inlet nozzle supplying H_2 gas from an electrolyser (Hydrogen South Africa Infrastructure, South Africa) at its maximum release rate of 138 NmL/min. The catalytic H_2 combustion into surrounding air increased the temperature progressively. This increase was recorded every second, over a period of 480 h, using a K-type thermocouple (RS PRO, South Africa).

2.4. CFD simulations

The 3D steady-state CFD simulations of the catalyst performance were performed using STAR-CCM + code supported with thermochemical data and reaction kinetics using the chemistry tool CHEMKIN. The computational domain consisted of the foams and the rectangular casing representing the recombiner's walls. The boundary conditions and computation domain mesh settings are presented in Fig. 2. To capture the real geometric features of the Pt/Al_2O_3-coated foam sample in the numerical study, a STL model was imported into the CFD code. The imported 3D geometry was subjected to re-tessellation and reparation to obtain a continuous surface with no self-intersected faces, edges and vertices. The 3D computational domain was created by inserting the repaired STL model into a rectangular recombiner channel that represents an actual experimental channel (Fig. 2). Then, 3D foam geometry was duplicated three times in the computational domain and subsequently subtracted from the fluid; then was re-imprinted in order to create an interface between the fluid and solid domains in the simulation. The repaired surface was volume meshed by using the same strategy as reported in previous work [29] (a polyhedral mesh was utilised). Mesh refinement was applied to the recombiner inlet and outlet, and around the catalytic section. Mesh independence was reached at a base size of 4 mm and all simulations discussed below were performed using the same base size. The total number of roughly 2 860 000 cells discretises the fluid and solid computational domains. The meshing parameters are summarised in Fig. 2.

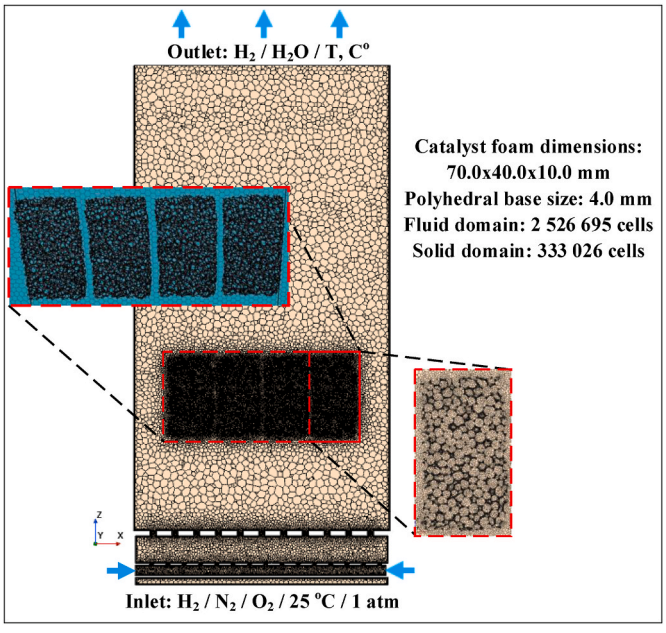

Fig. 2. Computational domain and boundary conditions of CFD model.

A realisable k-epsilon model with a two-layer approach based on Reynolds-averaged Navier–Stokes equations was used to simulate the turbulent flow inside the channel and through the foam pores [40,41]. A no-slip velocity condition was assumed at the walls and solid domains of the recombiner channel. An experimental inlet mass flow rate of 35.0 ± 0.2 g/min (corresponding to a gas inlet velocity of 10 m/s) and gas mixture composition of 2–6 vol% were set as the inlet boundary conditions. The governing equations were as follows (3D Cartesian coordinate system) [32,34,42,43].

Conservation of mass:

$$\frac{\partial \rho}{\partial t} + \nabla \bullet (\rho \vec{v}) = 0 \quad (3)$$

where ρ is the density (kg/m^3) and $\vec{v}$ is the continuum velocity (m/s).

Conservation of momentum:

$$\frac{\partial (\rho \vec{v})}{\partial t} + \nabla \bullet (\rho \vec{v} \otimes \vec{v}) = -\nabla \bullet \vec{\sigma} \quad (4)$$

where $\otimes$ denotes the outer product and $\vec{\sigma}$ is the stress tensor. For a fluid, $\vec{\sigma}$ can be calculated as

$$\vec{\sigma} = -p\boldsymbol{I} + \boldsymbol{T} \quad (5)$$

where p is the pressure (Pa), **T** is the viscous stress tensor, and **I** is the identity tensor. The viscous stress tensor **T** can be calculated as

$$\boldsymbol{T} = 2\mu^* \frac{1}{2}\left(\nabla \bar{v} + \nabla \bar{v}^T\right) - \frac{2}{3}(\mu \nabla^* \bar{v})\boldsymbol{I} \quad (6)$$

where μ is the dynamic viscosity (Pa.s) and $\bar{v}$ is the mean velocity.

Conservation of species:

$$\frac{\partial \rho Y_i}{\partial t} + \nabla \bullet (\rho U Y_i) = \nabla \bullet \left(J_i + \frac{\mu_t}{Sc_t} \nabla Y_i\right) + S_{Y_i} \quad (7)$$

where S_{Y_i} is the mass fraction source term, Y_i is the species mass fraction, U is the total internal energy (J), μ_t is the dynamic viscosity, J_i is the diffusive mass flux (kg/m^2/s), and Sc_t is the turbulent Schmidt number. The diffusive flux is calculated based on Fick's law

$$J_i = \rho D_{i,m} \nabla Y_i \quad (8)$$

where Y_i is the mass fraction of species i and $D_{i,m}$ is the diffusion coefficient of species i in the mixture (m^2/s). The Schmidt number function is available in STAR-CCM + for specifying molecular diffusivity of components in a mixture and is calculated as

$$Sc_t = \frac{\nu}{D_{i,m}} \quad (9)$$

where ν is the kinematic viscosity (m^2/s) and $D_{i,m}$ is the diffusion coefficient of species i in the mixture. In this study, a Schmidt number equal to 0.2 was used to influence the molecular diffusion coefficients in order to obtain reasonable accuracy of the computational results [29,44,45].

Conservation of energy:

$$\frac{\partial(\rho E)}{\partial t}+\nabla\bullet(\rho E\vec{v})=\vec{f_b}\bullet\vec{v}+\nabla\bullet(\vec{v}\times\vec{\sigma})-\nabla\bullet\vec{q}+S_E \quad (10)$$

where E is the total energy per unit mass (J/kg), $\vec{q}$ is the heat flux (W/m^2), and S_E is an energy source per unit volume (W/m^3).

The applied emissivity of the catalytic surface was $\varepsilon = 0.9$. The gas mixture ($H_2/O_2/N_2$) was assumed to be ideal. The components' thermophysical properties were obtained from the CHEMKIN material database. The rate constant was determined using the Arrhenius equation.

$$k_j = AT\exp\left(-\frac{E_a}{R_u T}\right) \quad (11)$$

where A is the pre-exponential factor (mol cm K s), T is the reaction temperature (K) and E_a is the activation energy (J/kmol) and R_u is the universal gas constant (J/kmol/K).

Table 2 summarises the detailed surface reaction kinetics mechanism utilised in order to simulate the catalytic H_2 recombination reaction [10,46].

The catalytic activity was assumed to occur only on Pt uniformly distributed on the surface of the section of the geometry representing the coated foam. A surface site density of $S_0 = 2.7 \times 10^{-8}$ kmol/m^2 was assumed [43]. A catalytic H_2 recombination reaction is associated with high thermal radiation, therefore, the surface-to-surface thermal radiation model was considered in CFD modelling [34]. In this study, the models of gravity force, thermal diffusion and external forces were not considered. The channel walls were assumed to be adiabatic.

3. Results and discussion

3.1. Characterisation

The textural properties related to the Pt/Al_2O_3-coated foams and geometric characteristics of the uncoated and coated foams are now reported and discussed. Their anticipated advantages on catalytic performance in the recombiner are briefly mentioned.

3.1.1. Textural properties

Fig. 3 shows SEM micrographs of the Pt/Al_2O_3-coated foams and EDS spectra of surfaces. The SEM micrographs of the foam struts confirmed that the Pt/Al_2O_3 catalyst was deposited over the entire surface of the Al foam. The surface of the catalyst layer was generally rugous and cracks were spotted at several struts on the foam (Fig. 3a). Some surface irregularities could have resulted from the removal of organic species (e.g. polyvinyl alcohol) during the calcination step after catalyst coating. This irregular surface morphology has the benefit of increasing the surface area of the catalyst deposited on the foam; foam-supported catalysts generally have a low gravimetric surface area [49]. The observed disadvantage of cracks in a catalyst washcoat layer is that they constitute weak points from which the catalyst tends to flake off the foam, especially at high catalyst loading or when the catalyst is subjected to intense mechanical or thermal stresses [22,50].

The EDS maps (Fig. 3b) confirmed the presence of Pt and Al_2O_3 particles on the entire surface of the catalyst washcoat. An even distribution of Pt on the surface of the washcoat is essential for maintaining high activity of the foam-based catalytic structure because Pt is the active metal in the PAR process. The presence of the morphological support (Al_2O_3) over the surface of the struts was expected as it is the most abundant constituent of the catalyst (~95 wt%). The high specific surface area of Al_2O_3 is an added advantage in the process. It maintains high dispersion of the Pt NPs over the surface whilst minimizing their agglomeration at prolonged reaction times [13,16].

TEM micrographs of the catalyst powders sampled from the washcoat layers of the foam samples before and after 480 h of reaction are shown in Fig. 4. It is evident that long-term exposure to the H_2 combustion process alters the Pt nanoparticle (NP) size. The average size of Pt NPs increased from 3.8 nm to 6.2 nm. Kozhukhova et al. [14] observed a smaller increase in particle size from 3.0 to 3.8 nm on their Pt catalyst supported on anodised Al plates exposed to 530 h combustion at ~160 °C. The higher combustion temperatures (~300 °C) reached during the long-term test in this study can explain the more pronounced agglomeration of Pt NPs. Nevertheless, the maximum NP size obtained is still within the size range of several catalysts reported in earlier literature, namely 5–20 nm [16,25,51].

The use of Al_2O_3 as morphological support could have prevented excessive sintering of the Pt NPs. In a study of catalytic H_2 combustion on Pt supported directly on stainless steel mesh, Du Preez et al. [39] obtained average Pt NP sizes of up to 120 nm after prolonged H_2 combustion reactions. The higher Pt mobility on the metal surface increases the tendency for agglomeration of Pt NPs, especially at high temperatures (>500 °C) or high moisture levels [18].

3.1.2. Geometric properties

Table 3 presents the geometric parameters calculated using CT results. The results revealed slight differences between the uncoated and coated foam samples. The coating process resulted in a 48% increase in the average strut diameter, which corresponds to an estimated average washcoat thickness of 75 μm. Such a relatively high value could be expected because 95% of the washcoat consists in the morphological support. Much thinner layers would be achieved if only the active phase (Pt) was deposited directly on the Al foam surface.

Tomograms of the uncoated and Pt/Al_2O_3-coated foam samples are presented in Fig. 5. The expected decreases in pore diameter and pore volume are a direct consequence of the increase in strut diameter from the catalyst coating process. In this study, the decrease in pore volume did not result in pore blocking because of the relatively large pores combined with small strut diameters. The 10 PPI foam used in this study has pores sufficiently large to accommodate relatively high catalyst amounts. Foams of higher pore density (e.g. 40 PPI) have the advantage of having a higher volumetric surface area due to the increased number of cells. However, they can easily be blocked during the catalyst coating step. This may result in a significant decrease in porosity and the occurrence of preferential pathways within the catalyst bed during the reaction. An unblocked foam-based catalyst support structure offers the benefit of improving mass transfer because of the high mixing and tortuosity increasing turbulence within the structure. Similarly, heat transfer is also improved by the contribution of conduction, convection and radiation in the heat-transfer mechanism [52].

Table 2
Heterogeneous mechanism of H_2/O_2 recombination on Pt. (Mechanism taken from a more detailed mechanism of H_2 oxidation on Pt from Deutschmann et al. [47,48]).

	Reactions	A[a]	E_a[b]	$S_{0,i}$[c]
1	$H_2 + 2Pt^{(s)} \rightarrow 2H^{(s)}$	0.0	0.0	0.046
2	$2H^{(s)} \rightarrow H_2 + 2Pt^{(s)}$	3.7×10^{21}	6.74×10^{7}	0.0
3	$O_2 + 2Pt^{(s)} \rightarrow 2O^{(s)}$	1.8×10^{21}	0.0	0.5
4	$O_2 + 2Pt^{(s)} \rightarrow 2O^{(s)}$	0.023	0.0	0.0
5	$2O^{(s)} \rightarrow O_2 + 2Pt^{(s)}$	3.7×10^{21}	2.132×10^{8}	0.0
6	$H_2O + Pt^{(s)} \rightarrow H_2O^{(s)}$	0.75	0.0	0.0
7	$H_2O^{(s)} \rightarrow H_2O + Pt^{(s)}$	1.0×10^{13}	4.03×10^{7}	0.0
8	$OH + Pt^{(s)} \rightarrow OH^{(s)}$	1.0	0.0	0.0
9	$OH^{(s)} \rightarrow OH + Pt^{(s)}$	1.0×10^{13}	1.928×10^{8}	0.0
10	$H^{(s)} + O^{(s)} = OH^{(s)} + Pt^{(s)}$	3.7×10^{21}	1.15×10^{7}	0.0
11	$H^{(s)} + OH^{(s)} = H_2O^{(s)} + Pt^{(s)}$	3.7×10^{21}	1.74×10^{7}	0.0
12	$OH^{(s)} + OH^{(s)} \rightarrow H_2O^{(s)} + O^{(s)}$	3.7×10^{21}	4.82×10^{7}	0.0

[a] Pre-exponential factor: A [mol cm K s].
[b] Activation energy: E_a [J/kmol].
[c] Sticking coefficient.

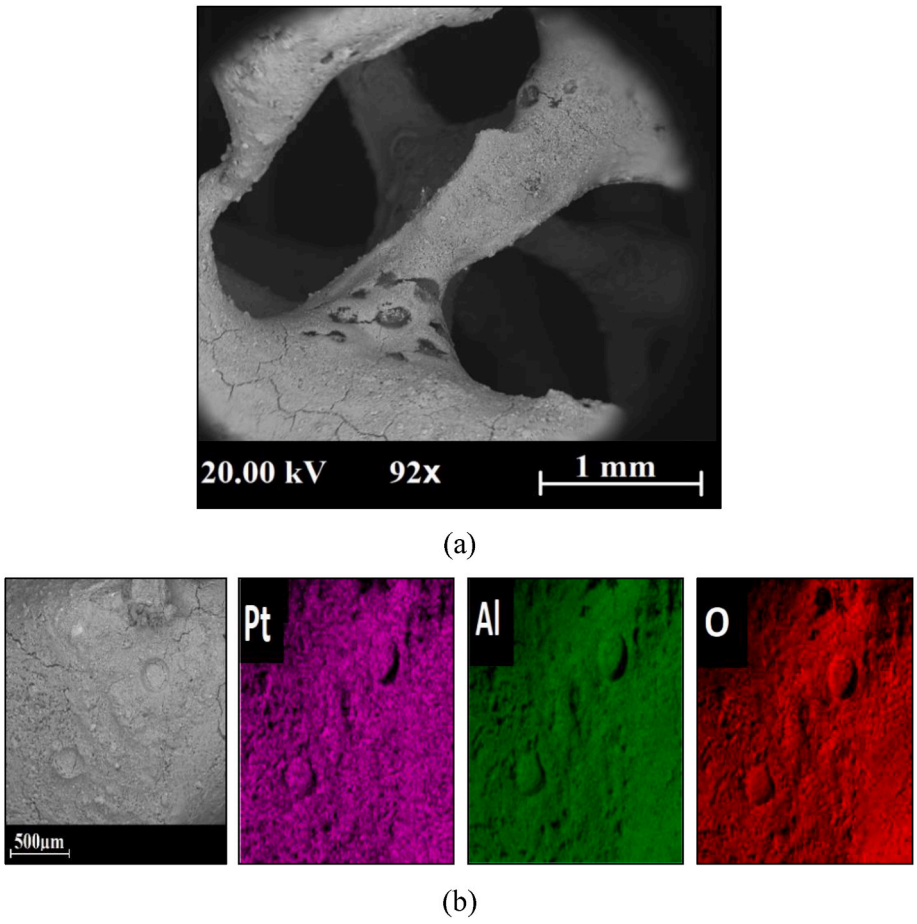

Fig. 3. (a) SEM micrograph of the coated foam, (b) EDS maps of the sample surface.

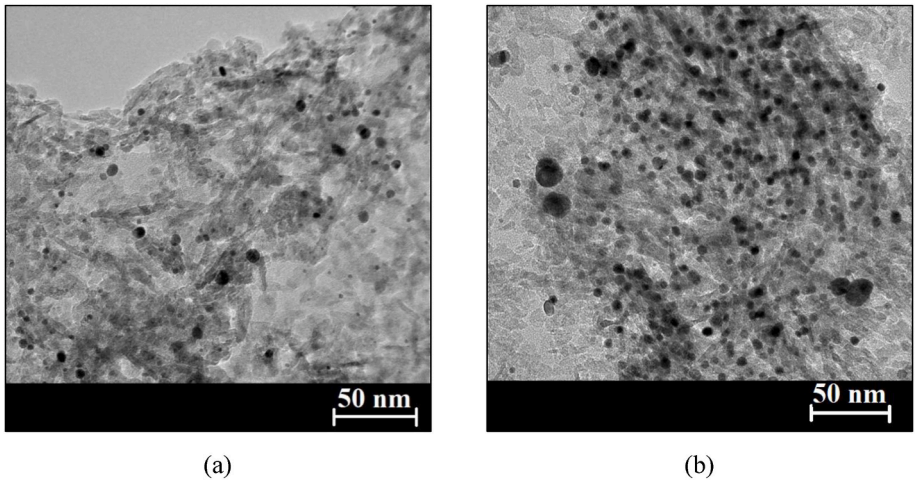

Fig. 4. TEM micrographs of Pt/Al_2O_3 catalyst extracted from (a) fresh foam and (b) used foam.

Table 3
Geometric properties of the 10 PPI Al foam used in this work.

Geometric property	Uncoated foam	Coated foam
Average strut diameter (mm)	0.31	0.46
Average pore diameter (mm)	4.19	3.37
Average pore volume (mm^3)	49.09	34.58
Volumetric surface area (m^2/m^3)	336.02	447.93

3.2. Catalytic activity tests

The effects of the inlet gas velocity and H_2 inlet concentrations on the performance of the Pt/Al_2O_3-coated foams in the recombiner are now reported. Pt/Al_2O_3-coated aluminium plates and pellet-based catalysts (for which the same amount of Pt/Al_2O_3 was used as on the coated foams) were also tested, at the same process conditions, for comparison. Average temperatures and temperatures at the hottest spots on the catalyst bed were also recorded to assess the operating conditions that

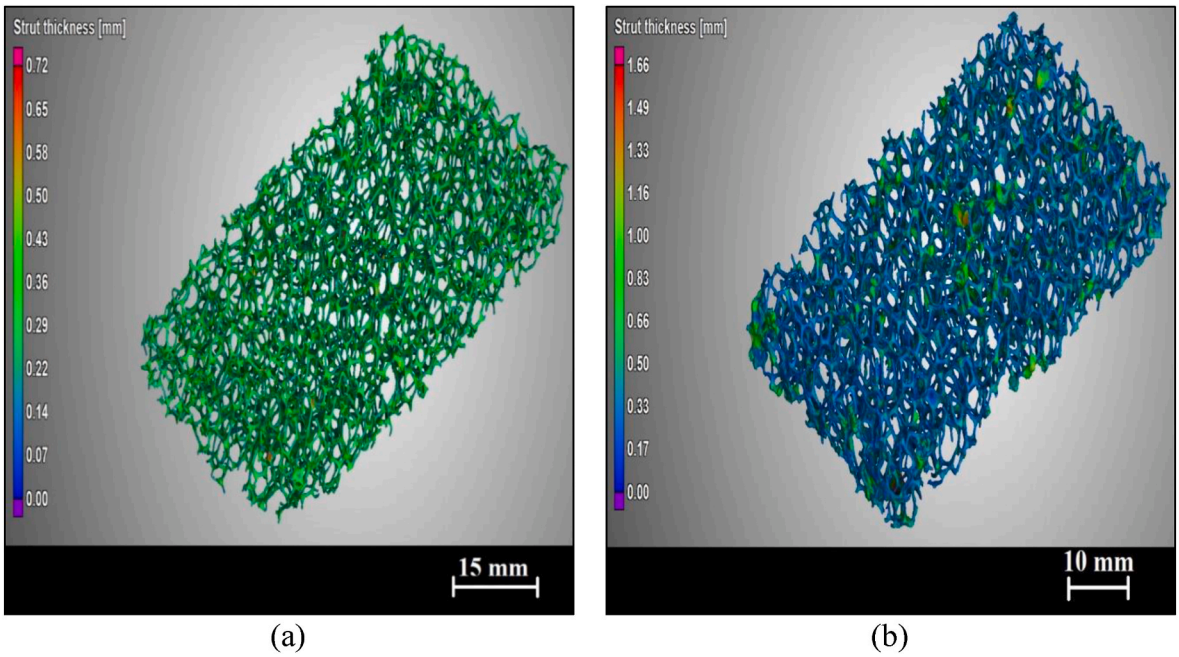

Fig. 5. Tomograms of 3D structures generated from CT scans of (a) uncoated foam and (b) coated foam.

posed the greatest safety risks. It was established that the foam-supported Pt/Al_2O_3 catalyst was able to withstand long-term continuous operation without showing signs of deactivation.

3.2.1. Effect of inlet gas velocity and H_2 concentration on the recombiner performance

The effects of the inlet gas velocity and inlet H_2 concentrations on the steady-state recombiner performance are shown in Fig. 6. To understand the overall recombination performance as a function of the inlet conditions, the H_2 conversions and surface temperatures were averaged over the four foam samples. During the PAR process, the exothermic H_2 combustion on the Pt/Al_2O_3 catalyst spontaneously commences at ambient temperature. As the reaction proceeds, more catalyst active sites are covered with H_2 and O_2 species, resulting in the occurrence of more H_2 combustion and heat release. This naturally increases the surface temperature of the foam – and the reaction kinetics – resulting in higher H_2 conversions, with further increases in the heat released [53]. Eventually, the combustion process transits from a kinetically controlled to a mass-transfer-controlled regime and a thermodynamic equilibrium is achieved at steady-state conditions [16]. The recombiner performances achieved at these steady-state conditions are strongly dependant on the supply of the gas mixture (reactants and inert N_2) and the reactant

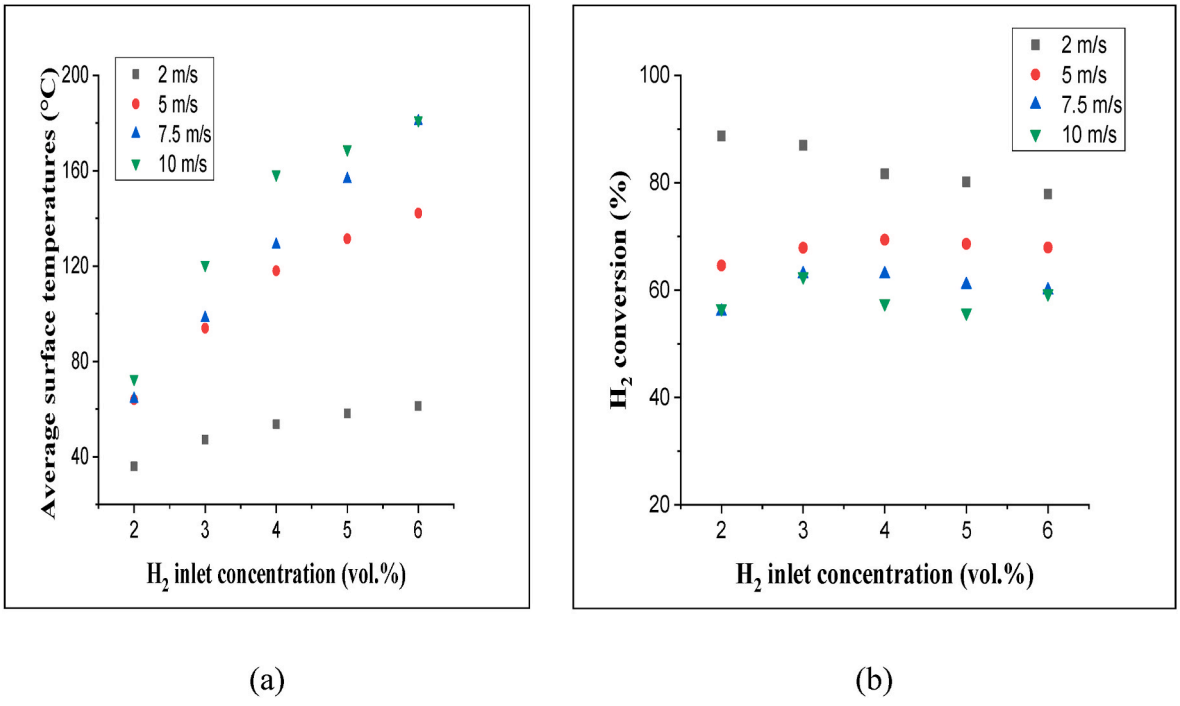

Fig. 6. Effects of inlet gas velocity and inlet H_2 concentration: (a) on the average surface temperature of the foams and (b) on the H_2 conversions.

consumption rate on the catalyst surface. The process outcome is therefore determined by the competing effects of reaction kinetic rates and mass transfer rate limitations at the gas–solid interface and in the gas phase.

Fig. 6a shows that the average steady-state surface temperatures of the four coated foam samples generally increases at higher inlet gas velocities. Increasing the surface temperatures causes an increase in the reaction rate [16,53]. However, the increase in combustion rate does not

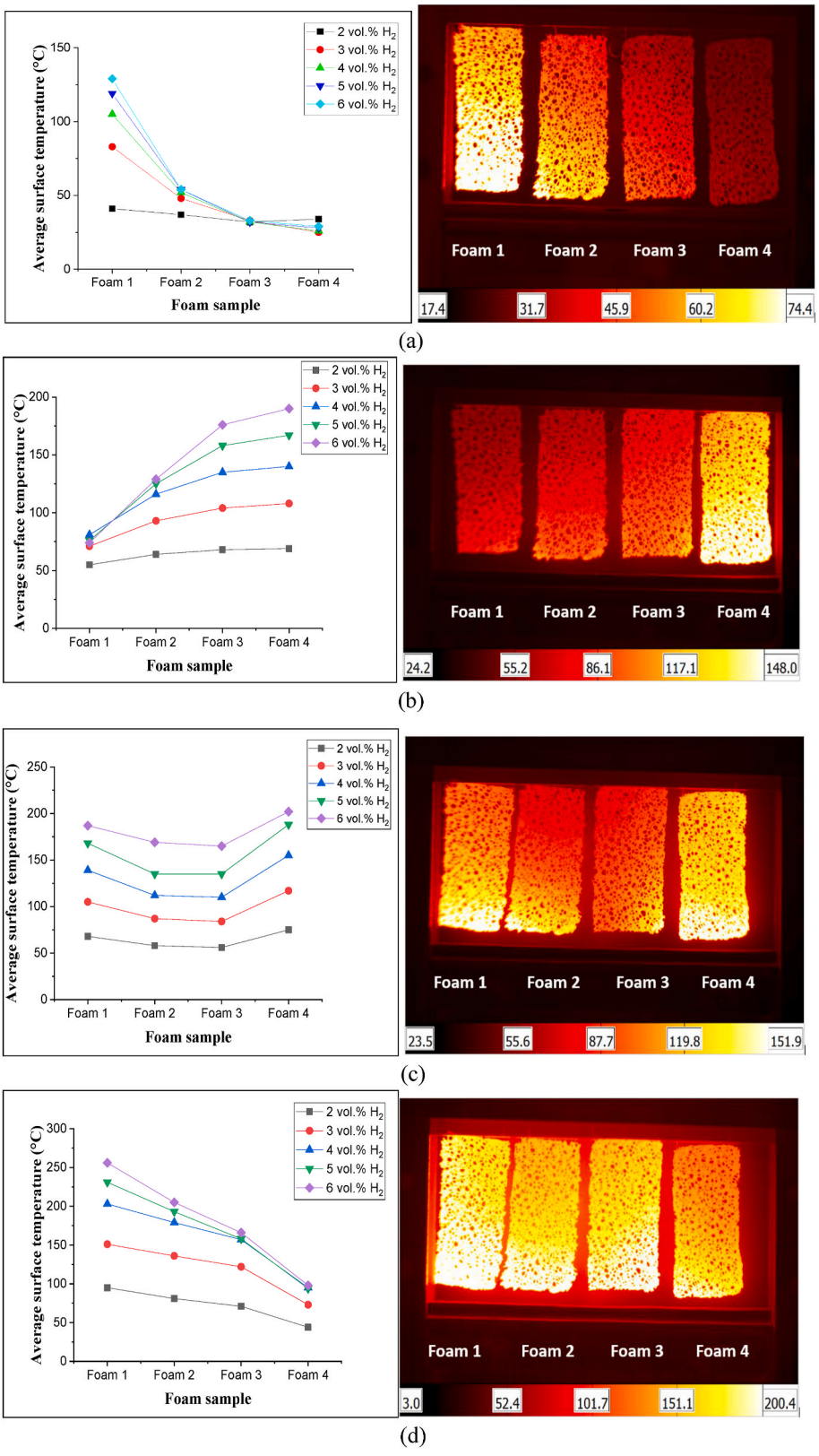

Fig. 7. Average temperatures obtained at inlet gas velocities of (a) 2 m/s, (b) 5 m/s, (c) 7.5 m/s and (d) 10 m/s, coupled with thermograms, obtained at inlet H_2 concentrations of 3 vol%.

cause an increase in H_2 conversions. From Fig. 6b it is evident that an increase in inlet gas velocity results in lower H_2 conversions. This can be attributed to the decrease in residence times on the catalyst surface [20,53]. Shorter residence times result in lower rates of mass transfer of reactants from the bulk of the fluid to the catalyst surface [16]. Consequently, more H_2 and O_2 leave the recombiner unreacted [18]. This, in turn, suggests that limitations in mass transfer rates prevail over kinetic rates at the experimental conditions investigated.

It is also evident from Fig. 6 that the recombiner performance is differently affected by H_2 concentrations at different inlet gas velocities. At a low gas inlet velocity of 2 m/s, as H_2 inlet concentrations increases from 2 to 6 vol%, the H_2 conversion decreases from 88.7% to 77.9%, while average steady-state temperatures increase from 36 to 61 °C. At higher H_2 inlet concentrations, more H_2 is fed to the foam surface. This results in higher rates of reaction, which then increase the catalyst surface temperature [54]. Despite this, the subsequent increase in combustion rate is not sufficiently high to compensate for the increasing amount of H_2 fed to the recombiner inlet at higher inlet H_2 concentrations. At higher inlet gas velocities (5–10 m/s), steeper increases in surface temperatures were observed with increasing H_2 inlet concentrations (Fig. 6a). Meanwhile, at the same conditions, the H_2 conversions remained almost constant (Fig. 6b). At these gas flow rates, the increase in H_2 consumption rates offset the increase in H_2 inflow at higher inlet concentrations.

Moreover, gas–solid and intermolecular gas-phase diffusions could limit the access of the reacting gas to the catalyst active sites [54], as also illustrated in Fig. 6. For equivalent amounts of incoming H_2, two different conversions can be obtained depending on the amount of inert gas (N_2) present in the feed. For instance, two gases fed at a velocity of 2 and 5 m/s and containing 5 and 2 vol% H_2 in air, respectively, introduce H_2 at the same rate in the recombiner but result in different conversions: 80.2 and 57.0%, respectively. Consequently, the recombiner performed better when removing H_2 from slow leaks of relatively high H_2 concentrations than from rapid leaks of low H_2 concentrations.

3.2.2. Temperature profiles in the foam-based recombiner

Arguably, one of the greatest practical challenges in a PAR set-up is to establish the optimum location at which maximum H_2 conversion will be achieved, preferably at the lowest temperature possible. Fig. 7 reports the average temperatures obtained on each of the four Pt/Al_2O_3-coated foams at different inlet gas flow velocities and H_2 concentrations. The thermograms illustrate the temperature profiles for the four foam samples at selected inlet conditions. There are several possible reasons for the different temperature profiles across the catalyst bed, including an uneven gas distribution inside the recombiner due to different unpredictable flow patterns of the gas entering the reaction zone [10], or a possible higher concentration of the catalytically active metals at one particular spot on the catalyst bed (i.e. a non-uniform catalyst washcoat layer) [14]. This last possibility is unlikely, because the profiles in Fig. 7 show that the hottest foams are not the same at the different flow conditions. At inlet gas conditions of 7.5 m/s, the temperature profiles were found to be the most uniform. In the case of accidental leaks in large-scale settings, even gas distribution is very unlikely to occur; hence the recombiner positioning is an important optimisation parameter in the mitigation of risks related H_2 leaks in confined spaces.

The highest temperatures were obtained at the base of the foams. A maximum temperature of 393 °C was measured on Foam 1 at the highest H_2 inlet concentration and inlet gas velocity. The average surface temperature of Foam 1 was 252 °C. This confirms the heat dissipation capability of foam-based catalyst beds, attributed to their high thermal conductivity and high porosity. Heat transfer occurs by conduction through the metal struts as well as convective and radiative heat transfer through the foam's pores [52,53,55]. Relatively large amounts of inert N_2 and unreacted species flow through the foams. These species that enter the recombiner at ambient temperature contribute to cooling the surface of the coated foams. The maximum temperatures obtained on the coated foams were generally still <585 °C—the temperature for spontaneous combustion of H_2 within its flammability limits.

3.2.3. Effect of configuration of the catalyst region on the recombiner performance

Fig. 8 shows the results of a comparison of the performances of the Pt/Al_2O_3-coated foams, coated plates and pellet-based catalysts. Major differences between the three configurations include the volume occupied by the catalyst bed and the exposed catalytic surface area in the recombiner. These differences have an impact on the gas–solid mass transfer rates. The high macro-porosity of the foam-based bed causes it to occupy a larger volume in the recombiner than the plates do, and especially larger than the pellets. This contributes to the higher exposure of H_2 gas on the catalyst surface despite its high dilution in the relatively large amount of N_2 in the incoming gas. For instance, a higher H_2 conversion was achieved in the foam-based catalytic recombiner when a 2 vol% H_2 gas was fed at a velocity of 2 m/s (Fig. 8a). The spontaneous combustion of H_2 at very low concentrations is of great practical importance because a recombiner should be able to prevent accumulation of H_2 by oxidising it within the first instants of slow accidental leaks in confined spaces.

At the same inlet gas velocity of 2 m/s, and as the H_2 inlet concentrations increases, the performance advantage of the foams is lost. As more H_2 is fed to the recombiner, more H_2 is exposed to the catalyst surface, thus the H_2 conversion on plates and pellets increases, as expected, until the point at which gas–solid mass transfer limitations prohibit higher conversions (Fig. 8a). At higher inlet gas flow rates (Fig. 8b–d), the pellet-based configuration proves to be less suitable for high-velocity leaks than the foams and plates. The amount of pellets loaded in the recombiner should be increased significantly in order to improve their efficiency. One way to improve the performance of pellets is to use a catalyst of lower Pt loading (e.g. 0.2 wt% Pt/Al_2O_3) dispersed on more Al_2O_3 pellets. This increase in dispersion will inevitably require larger amounts of Al_2O_3 to be used in the recombiner. Additional information on the performance of the plate-based and pellet-based recombiners can be found in the Supplementary data.

3.2.4. Catalyst durability tests

For safety applications, the recombiner should be equipped with a catalytic system characterised by short initiation times and high stability upon prolonged exposure to streams of H_2 gas. In the present work, the foam-supported Pt/Al_2O_3 catalyst was exposed to a constant H_2 flow of 138 mL/min for 480 h. Fig. 9 shows the maximum temperature achieved during the test. On fresh foam-supported Pt/Al_2O_3, H_2 combustion was initiated at ambient temperature (~24 °C) after a time of 35 s. The combustion temperature subsequently increased over a period of ~215 s before steady state was achieved (Fig. 9a). In an earlier study performed at the same flow conditions [14], H_2 combustion on a Pt catalyst supported on anodised aluminium oxide was initiated within 27 s and stabilised slowly after ~500 s. The rapid heating observed in the present study was attributed to the relatively low amount of material (0.2 g Pt/Al_2O_3 and 0.5 g Al foam) and the high thermal conductivity of the Al foam (237 W/m/K). The catalyst bed could therefore heat up much faster. This can also be seen in the higher combustion temperature achieved (~300 °C vs 163 °C in Ref. [14]) once steady state was reached. Almost constant catalytic activity was maintained for a period of >480 h on stream (Fig. 9b). This is a preliminary indication of the stability of the 5 wt% Pt/Al_2O_3 supported on Al foam.

The fluctuations seen in the temperature profile in Fig. 9b were attributed to insufficient thermal insulation, which caused the reactor to be subjected to the environmental fluctuations in the laboratory [13]. Some water vapour condensation was observed around the reactor wall and towards the reactor outlet (these areas were colder than the reactor inlet where the reaction takes place). These droplets caused an increase in relative humidity inside the reactor, even causing some water droplets to fall on the catalyst surface, despite the precaution taken to prevent

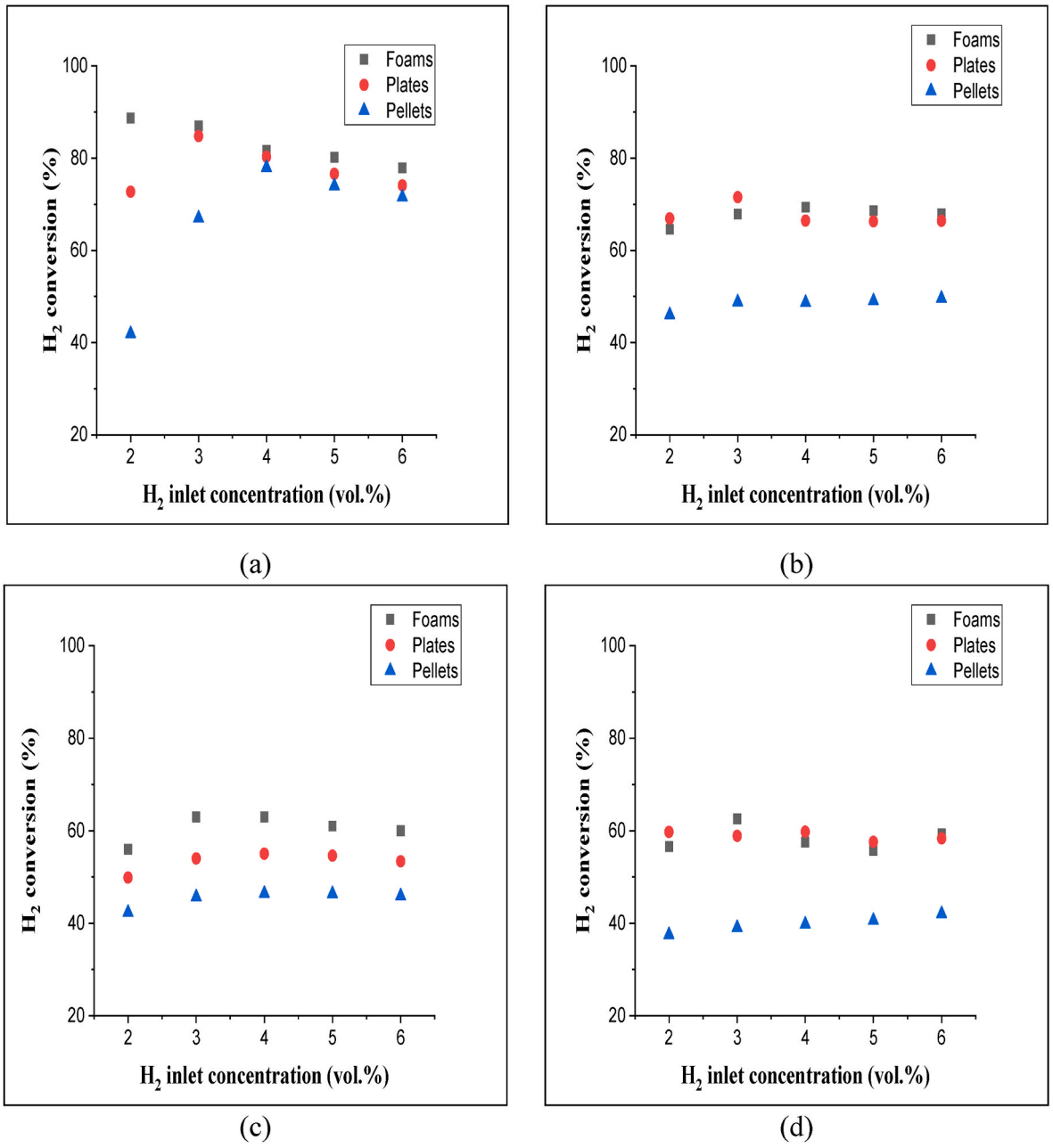

Fig. 8. Effect of support structure configuration and inlet H_2 concentration on the H_2 conversion at inlet gas velocities of (a) 2 m/s, (b) 5 m/s, (c) 7.5 m/s and (d) 10 m/s.

interference with the catalyst surface.

The catalyst subjected to the long-term test was allowed to cool to room temperature and was later exposed to the same experimental conditions as the freshly prepared catalyst. The initiation and stabilisation times were increased by ~15 and 95 s, respectively (Fig. 9a). This slight change in catalytic behaviour is an indication of possible changes in the textural properties of the catalyst [11]. TEM analysis of the used catalyst revealed an increase in Pt NPs (Fig. 4). Nevertheless, the observed maximum temperatures were similar on both the used and fresh catalyst bed.

4. CFD modelling results

The catalytic H_2 recombination reaction is highly exothermic. The heat released is transferred through conduction within the struts, convection in the fluid domain and thermal radiation in the foam pores. These three mechanisms of heat transport are included in the conjugated heat transport model [56]. It was found that thermal radiation plays a particularly significant role in the heat transport model. As illustrated in Fig. 10, the CFD model validation shows that neglecting the thermal radiation model in CFD simulation of catalytic recombination results in overprediction of the catalyst temperature profile, worsening as the inlet H_2 concentration increases. This has been demonstrated in a plate-type recombiner catalyst by Meynet et al. [57]. Sinn et al. [58] demonstrated similar deviations in their results of a study of combustion on foam catalysts. The maximum calculated temperature of the catalytic foam was overpredicted by ~120 °C at 6 vol% of inlet H_2.

Fig. 11 shows plots of the simulated velocity, H_2 mole fraction, H_2O mole fraction and temperature profiles along the middle of the channel and centre of catalytic foams at 4 vol% of inlet H_2. As reported in a previous study by Malakhov et al. [29], at the inlet mass flow rate of 35.0 ± 0.2 g/min the flow velocity is distributed uniformly throughout

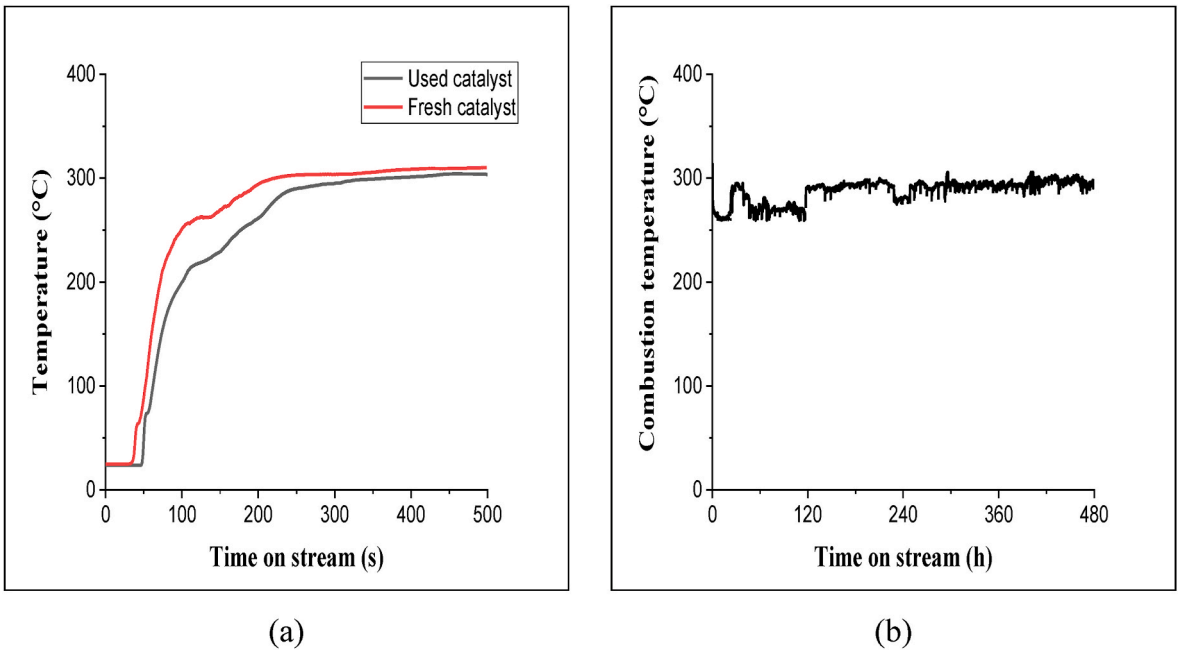

Fig. 9. Temperature profiles recorded on the surface a coated foam (a) during the initial 500 s and (b) over a period of 480 h on stream.

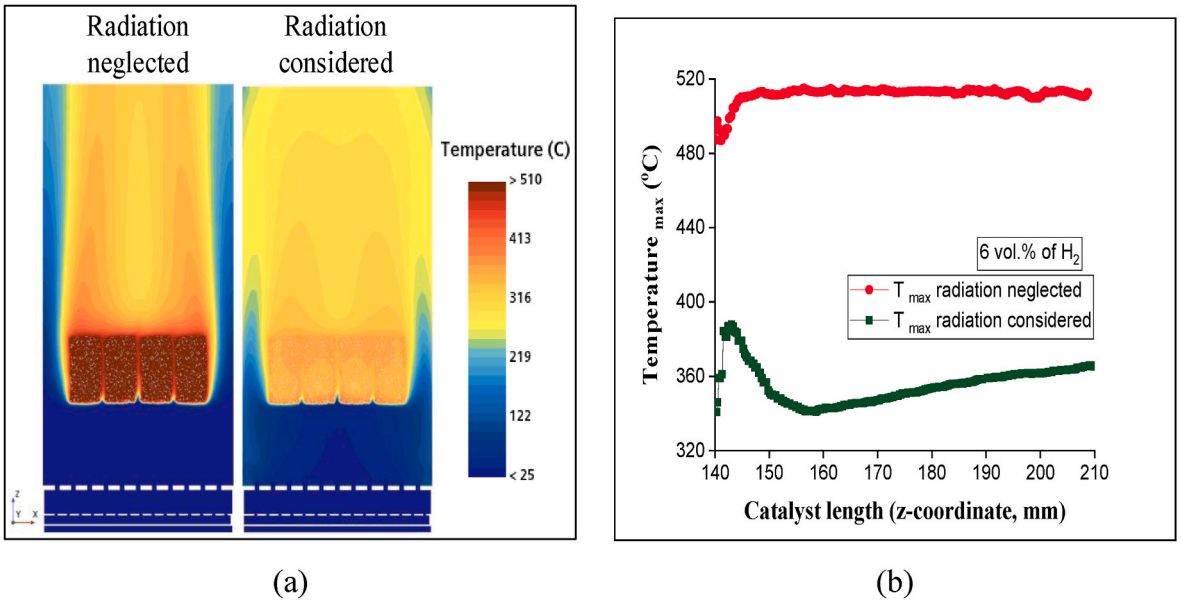

Fig. 10. Comparison between temperature profiles obtained at an inlet gas flow rate of 35.0 ± 0.2 g/min (inlet velocity ~10 m/s) and concentration 6 vol% H_2 in simulations: (a) including the radiation model and (b) excluding the radiation model.

the recombiner channel and the catalyst area in the middle (Fig. 11a and b). Two zones of high turbulence vortex can be seen on the right- and left-hand sides at the bottom of the channel below the catalyst foam. These two turbulent zones cause the flow to decrease, resulting in a slightly lower catalyst temperature of foams 1 and 4 (Fig. 11e).

Fig. 11c displays the H_2 distribution profile along the recombiner channel, indicating near-complete recombination of H_2 on the catalyst surface and within a small area around the foam. However, a certain amount of H_2 slips away unreacted on the catalyst surface and escapes through the outlet boundary of the channel, resulting in incomplete H_2 conversion.

Fig. 11d presents a typical steady-state profile of the H_2O. It demonstrates that ~4.04 vol% of H_2O is generated during the catalytic H_2 recombination reaction at 4 vol% of inlet H_2. A similar profile of reaction products has been published by Malakhov et al. [10]. Fig. 11e illustrates the temperature profile along the channel length and the catalyst surface. A maximum catalyst temperature of 293 °C was observed at the bottom edge of all four of the foam samples at 4 vol% of inlet H_2, corresponding to the position of higher H_2 concentrations and flow rates. The simulated positions and magnitudes of temperature maxima were found to be in good agreement with experimental results.

Fig. 12 shows the H_2 and H_2O concentration profiles together with a comparison of the simulated and experimental catalyst temperatures along the length of the catalytic foam, obtained at an inlet gas flow rate of 35.0 ± 0.2 g/min and inlet H_2 concentrations of 2% and 4 vol%. The H_2 profiles demonstrate a near-complete H_2 conversion along the length

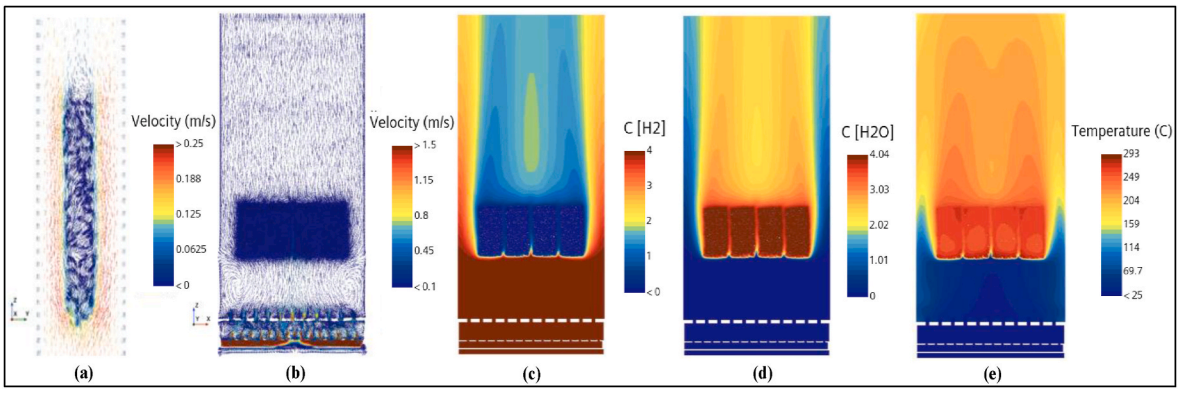

Fig. 11. Calculated profiles of the velocity, temperature, and concentration of H_2 and H_2O (inlet gas flow rate 35.0 ± 0.2 g/min, inlet H_2 concentration 4 vol%).

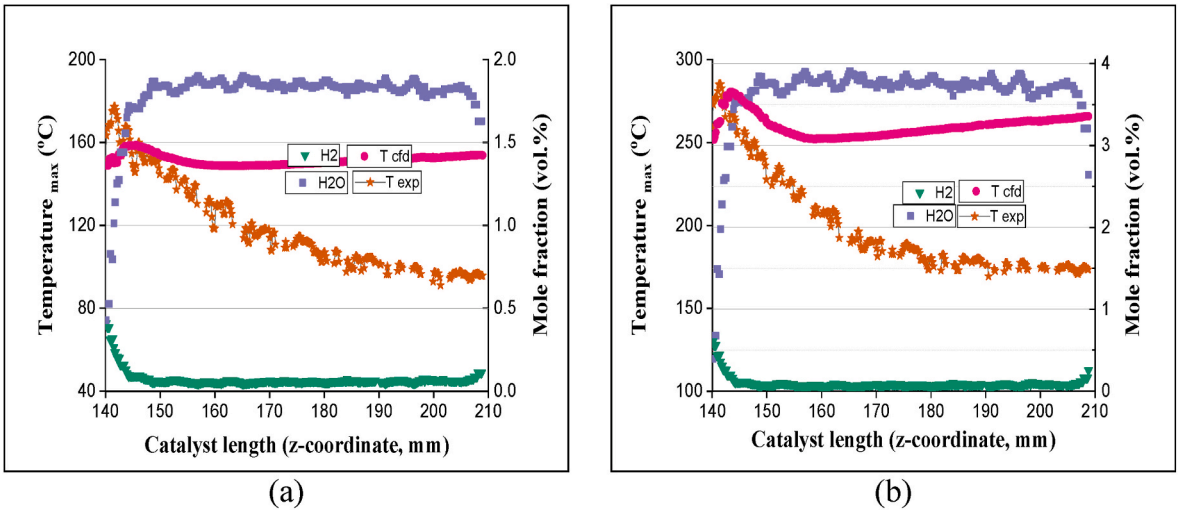

Fig. 12. H_2 and H_2O mole concentration profiles together with experimental and simulated temperatures obtained at an inlet gas flow rate of 35.0 ± 0.2 g/min and inlet H_2 concentrations of (a) 2 vol% H_2 and (b) 4 vol% H_2.

of the catalytic foam in both cases. The H_2 concentrations at the bottom edge of the foam are about 0.5 and 0.65 vol%, respectively. These low H_2 concentrations confirm that most H_2 conversion occurs towards the bottom edge of the foam. Therefore, this section heated up faster than the remaining part of the catalytic structure. Nearly complete H_2 conversion was achieved within the first 10 mm from the bottom edge of the foam. At the last few millimetres above the foam, the slight increase in H_2 concentration and temperature are due to the higher velocity of free stream that comes up around the foam (see Fig. 11).

As mentioned above, at the bottom edge of the foam, the numerically simulated maximum catalyst temperatures are in good agreement with experimental values at all the inlet H_2 concentrations considered here. However, along the foam length, the temperature profiles are systematically different (Fig. 13). Both the experimental and simulation profiles decrease after the maximum at the bottom edge until the upper edge of the foam, while the experimental temperature decreases steeply and then stabilises to linear after 30 mm of its length; the numerically simulated temperature slightly decreases for the first 15 mm after the maximum and then increases towards the top edge of the foam without reaching the maximum temperature of the bottom edge. Such a steep down-slope profile indicates heat loss along the catalyst length due to the experimental channel not being truly adiabatic.

The catalyst demonstrates a lower temperature of ~150 °C at 2 vol% of H_2. The temperature increases as the inlet H_2 concentration increases, resulting in 235 °C, 295 °C, 340 °C and 395 °C at 3, 4, 5 and 6 vol% of inlet H_2, respectively. It was observed that the deviation between

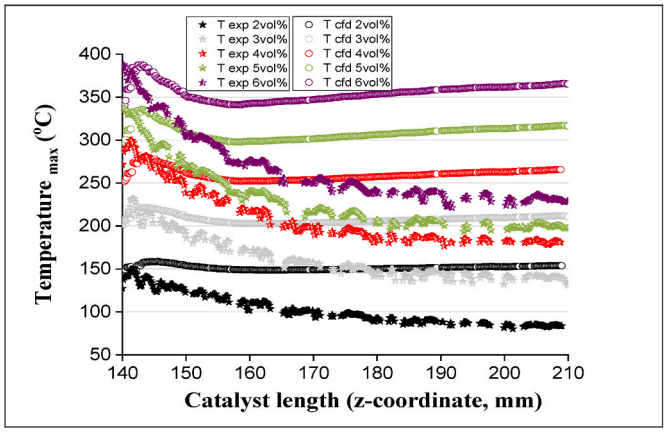

Fig. 13. Comparison of the experimental and simulation temperature profiles along the foam length (z-coordinate, at an inlet gas flow rate of 35.0 ± 0.2 g/min).

experimental and simulated temperature increased with increasing H_2 concentrations [29]; however, the overall numerically simulated trend demonstrates a reasonable prediction of experiment data.

A comparison of the experimental and simulated H_2 conversions obtained on the foam-based catalyst is displayed in Fig. 14, for all

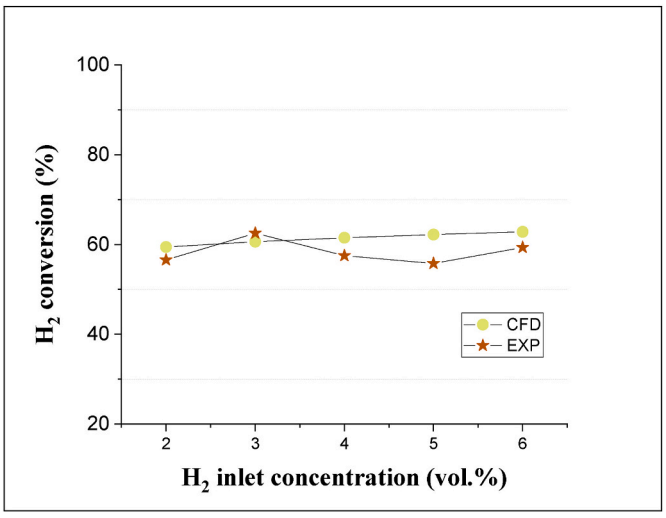

Fig. 14. Comparison of the experimental and simulated H_2 conversion at an inlet gas flow rate of 35.0 ± 0.2 g/min (inlet gas velocity 10 m/s).

considered cases mentioned. Results show that the average experimental and simulated conversions agreed reasonably well. Both cases show that the inlet H_2 concentrations did not significantly affect H_2 conversion.

5. Conclusions

Catalytic H_2 combustion tests were conducted in a bench-scale recombiner containing an in-house prepared catalyst (5 wt% Pt/Al_2O_3) coated on commercial Al foams. SEM images and EDS spectra of the coated foams revealed a uniform distribution of the catalyst on the entire Al foam surface. This confirms the suitability of slurry coating as catalyst deposition procedure on a metal foam used for PAR. TEM micrographs showed that long-term catalytic activity increased the particle size from 3.8 to 6.2 nm. However, this increase did not negatively impact the catalytic performance. The foam-supported catalyst maintained a constant activity for more than 480 h on stream.

A comparison between the performances of the foam-, plate-supported and pellet catalysts indicated that the foam-supported catalyst bed has the potential to mitigate risks similar to that achieved with coated plates, and even more so with catalyst pellets, during long periods of exposure to H_2. At the operating conditions investigated in this study, H_2 conversions of 57–89%, 50–87% and 37–78% were obtained on the foam-, plate-supported and pellet catalysts respectively. This suggested that the geometric configuration had a significant effect on the H_2 conversions obtained at different gas flow conditions, i.e. inlet gas velocity, H_2 concentration and gas distribution. The geometric configuration affected the relative importance of kinetic and mass transfer rates on the catalyst surface. Increasing the volumetric surface area of the catalytic system has the potential to improve the overall H_2 conversion capability of the recombiner.

The uneven temperature profiles observed during the catalytic tests were attributed to the unpredictable gas flow distribution in the recombiner. The profiles revealed the importance of selecting a suitable position for the catalytic bed in the recombiner. Nevertheless, the maximum temperatures obtained at all conditions were much lower than 585 °C, temperature at which gas phase combustion can occur.

CFD simulations revealed important insights into the transport phenomena within the Pt/Al_2O_3-coated foams during the PAR process. The simulations demonstrated that neglecting the thermal radiation model can significantly overpredict catalyst temperatures, as evidenced by past studies in plate-type recombiners and on foam-supported catalysts used for CO combustion. The calculated maximum temperatures obtained at the bottom edge of the foams – near the reactor inlet – corresponded well with experimental data. However, evident profile differences were observed elsewhere along the catalyst length. Experimental results indicated a steeper temperature decline compared to simulations, attributed to heat loss under the non-adiabatic experimental conditions. The model also showed that near-complete H_2 conversions were obtained within the catalytic foam region. This suggests that the unconverted H_2 is concentrated in the areas of the recombiner that are not occupied by the foam. Simulated H_2 conversions were also in relatively good agreement with experimental calculations, confirming the validity of the kinetic and transport models used in the calculations.

Overall, this investigation confirms the effectiveness of a foam-supported recombiner for the PAR process. However, some uncertainty remains regarding the benefits of foam-supported catalysts for PAR applications. The following are suggested as topics for further experimental and modelling studies: determinations of the effects of the pore density, the thickness of the washcoat layer, the size and position of the catalytic foam in the recombiner.

CRediT authorship contribution statement

Kyatsinge Cédric Musavuli: Writing – review & editing, Writing – original draft, Visualization, Validation, Resources, Methodology, Investigation, Formal analysis, Data curation, Conceptualization. **Alexander Malakhov:** Writing – review & editing, Visualization, Validation, Supervision, Software, Resources, Methodology, Investigation, Formal analysis, Data curation. **Raymond Cecil Everson:** Writing – review & editing, Supervision, Project administration, Formal analysis, Data curation. **Alina Kozhukhova:** Writing – review & editing, Visualization, Validation, Resources, Methodology, Investigation, Formal analysis, Data curation, Conceptualization. **Phillimon Modisha:** Writing – review & editing, Supervision, Project administration, Formal analysis, Data curation, Conceptualization. **Dmitri Bessarabov:** Writing – review & editing, Supervision, Resources, Project administration, Funding acquisition, Data curation, Conceptualization.

Declaration of competing interest

The authors declare that they have no known competing financial interests or personal relationships that could have appeared to influence the work reported in this paper.

Acknowledgements

This work was supported by the Department of Science and Innovation (KP5 program), HySA Infrastructure, South Africa, through their financial support, and National Research Foundation of South Africa through their grant [PSTD2203291140]. The authors' gratitude is expressed to Mr. Dance Mabu for the SEM/EDS analysis (North-West University, Potchefstroom, South Africa), Ms. Carlyn Wells for the CT scans of the metal foams (Stellenbosch University, Stellenbosch, South Africa), and Dr. Solly Motaung and Ms. Rirhandzu Rikhotso-Mbungela for their assistance with catalyst characterisation (CSIR, Pretoria, South Africa). The authors also thank the Centre for High Performance Computing (CHPC) (South Africa) for computational resources used in this study.

Appendix A. Supplementary data

Supplementary data to this article can be found online at https://doi.org/10.1016/j.ijhydene.2024.11.116.

References

[1] Wang W, Yuan B, Sun Q, Wennersten R. Application of energy storage in integrated energy systems — a solution to fluctuation and uncertainty of renewable energy. J Energy Storage 2022;52:104812. https://doi.org/10.1016/j.est.2022.104812.

[2] Sayed E, Olabi A, Alami A, Radwan A, Mdallal A, Rezk A, Abdelkareem M. Renewable energy and energy storage systems. Energies 2023;16(3):1415. https://doi.org/10.3390/en16031415.

[3] Chibani A, Boucetta C, Merouani S, Belahmadi E, Laidoudi H, Bessaïh R. Performance investigation of metal foam coupled to phase change material as coolant of photovoltaic concentrator systems: optimization and electrical efficiency analysis. J. Eng. Res. 2024;S2307187724002153. https://doi.org/10.1016/j.jer.2024.07.022.

[4] Chibani A, Dehane A, Merouani S, Bougriou C, Guerraiche D. Melting/solidification of phase change material in a multi-tube heat exchanger in the presence of metal foam: effect of the geometrical configuration of tubes. Energy Storage Saving 2022;1(4):241–58. https://doi.org/10.1016/j.enss.2022.07.004.

[5] Egeland-Eriksen T, Hajizadeh A, Sartori S. Hydrogen-based systems for integration of renewable energy in power systems: achievements and perspectives. Int J Hydrogen Energy 2021;46(63):31963–83. https://doi.org/10.1016/j.ijhydene.2021.06.218.

[6] Stenina I, Yaroslavtsev A. Modern technologies of hydrogen production. Processes 2022;11(1):56. https://doi.org/10.3390/pr11010056.

[7] IEA. The future of hydrogen energy. 2019. Accessed 19 July 2024, https://iea.blob.core.windows.net/assets/9e3a3493-b9a6-4b7d-b499-7ca48e357561/The_Future_of_Hydrogen.pdf.

[8] Rahbari A, Homayoonfar S, Valizadeh E, Aligoodarz MR, Toghraie D. Effects of micro-combustor geometry and size on the heat transfer and combustion characteristics of premixed hydrogen/air flames. Energy 2021;215:119061. https://doi.org/10.1016/j.energy.2020.119061.

[9] Kirillov Igor A. Passive autocatalytic recombiners as explosion prevention and mitigation tool in hydrogen energy and transport infrastructures. Chem. Eng. Trans. 2022;90:127–32. https://doi.org/10.3303/CET2290022.

[10] Malakhov AA, Du Toit MH, Du Preez SP, Avdeenkov AV, Bessarabov DG. Temperature profile mapping over a catalytic unit of a hydrogen passive autocatalytic recombiner: an experimental and computational fluid dynamics study. Energy Fuel 2020;34(9):11637–49. https://doi.org/10.1021/acs.energyfuels.0c01582.

[11] Kozhukhova AE, Du Preez SP, Bessarabov DG. Development of Pt–Co/Al_2O_3 bimetallic catalyst and its evaluation in catalytic hydrogen combustion reaction. Int J Hydrogen Energy 2024;51:1079–96. https://doi.org/10.1016/j.ijhydene.2023.09.119.

[12] IAEA. Mitigation of hydrogen hazards in severe accidents in severe accidents in nuclear power plants. Available at. 2011. Accessed 19 July 2024, https://www-pub.iaea.org/mtcd/publications/pdf/te_1661_web.pdf.

[13] Du Preez S, Kozhukhova A, Bessarabov D. Catalytic hydrogen combustion using platinum supported on anodized aluminium oxide adhered to metallic aluminium. S Afr J Chem 2022;76:31–7. https://doi.org/10.17159/0379-4350/2022/v76a06.

[14] Kozhukhova AE, Du Preez SP, Malakhov AA, Bessarabov DG. A thermally conductive Pt/AAO catalyst for hydrogen passive autocatalytic recombination. Catalysts 2021;11(4):491. https://doi.org/10.3390/catal11040491.

[15] Zanoni MAB, Gardner L, Gnanapragasam N, Liang Z. Application of passive autocatalytic recombiners for hydrogen mitigation: 2D numerical modeling and experimental validation. Int J Hydrogen Energy 2024;57:39–51. https://doi.org/10.1016/j.ijhydene.2023.12.192.

[16] Kim J, Yu J, Lee S, Tahmasebi A, Jeon C-H, Lucas J. Advances in catalytic hydrogen combustion research: catalysts, mechanism, kinetics, and reactor designs. Int J Hydrogen Energy 2021;46(80):40073–104. https://doi.org/10.1016/j.ijhydene.2021.09.236.

[17] Singh SA, Vishwanath K, Madras G. Role of hydrogen and oxygen activation over pt and Pd-doped composites for catalytic hydrogen combustion. ACS Appl Mater Interfaces 2017;9(23):19380–8. https://doi.org/10.1021/acsami.6b08019.

[18] Du Preez SP, Jones DR, Warwick MEA, Falch A, Sekoai PT, Mota Das Neves Quaresma C, Bessarabov DG, Dunnill CW. Thermally stable Pt/Ti mesh catalyst for catalytic hydrogen combustion. Int J Hydrogen Energy 2020;45(33):16851–64. https://doi.org/10.1016/j.ijhydene.2020.04.112.

[19] Gancarczyk A, Sindera K, Iwaniszyn M, Piątek M, Macek W, Jodłowski PJ, Wroński S, Sitarz M, Łojewska J, Kołodziej A. Metal foams as novel catalyst support in environmental processes. Catalysts 2019;9(7):587. https://doi.org/10.3390/catal9070587.

[20] Jo S, Jin J, Kwon S. The preparation of a metal foam support of Pt/Al_2O_3 for combustion of hydrogen. Catal Today 2010;155(1–2):45–50. https://doi.org/10.1016/j.cattod.2009.04.021.

[21] Kapteijn F, Moulijn JA. Structured catalysts and reactors – perspectives for demanding applications. Catal Today 2022;383:5–14. https://doi.org/10.1016/j.cattod.2020.09.026.

[22] Montebelli A, Visconti CG, Groppi G, Tronconi E, Cristiani C, Ferreira C, Kohler S. Methods for the catalytic activation of metallic structured substrates. Catal Sci Technol 2014;4(9):2846–70. https://doi.org/10.1039/C4CY00179F.

[23] Jin J, Kwon S. Microcatalytic combustion of H_2 on Pt/Al_2O_3-coated nickel foam. Combust Sci Technol 2009;181(2):211–25.

[24] Fumey B, Stoller S, Fricker R, Weber R, Dorer V, Vogt UF. Development of a novel cooking stove based on catalytic hydrogen combustion. Int J Hydrogen Energy 2016;41(18):7494–9. https://doi.org/10.1016/j.ijhydene.2016.03.134.

[25] Fernández A, Arzac GM, Vogt UF, Hosoglu F, Borgschulte A, Jiménez De Haro MC, Montes O, Züttel A. Investigation of a Pt containing washcoat on SiC foam for hydrogen combustion applications. Appl Catal B Environ 2016;180:336–43. https://doi.org/10.1016/j.apcatb.2015.06.040.

[26] Kozhukhova AE, Du Preez SP, Shuro I, Bessarabov DG. Preparation of a cartridge-type Pt/Al_2O_3 catalyst using a sputter deposition method for catalytic hydrogen combustion. Energy Fuel 2022;36(22):13911–23. https://doi.org/10.1021/acs.energyfuels.2c02584.

[27] Halouane Y, Dehbi A. CFD simulations of premixed hydrogen combustion using the eddy dissipation and the turbulent flame closure models. Int J Hydrogen Energy 2017;42(34):21990–2004. https://doi.org/10.1016/j.ijhydene.2017.07.075.

[28] Mayrhofer M, Koller M, Seemann P, Bordbar H, Prieler R, Hochenauer C. MILD combustion of hydrogen and air – an efficient modelling approach in CFD validated by experimental data. Int J Hydrogen Energy 2022;47(9):6349–64. https://doi.org/10.1016/j.ijhydene.2021.11.236.

[29] Malakhov AA, Avdeenkov AV, Du Toit MH, Duong QH, Bessarabov DG. Numerical and experimental analysis of cylindrical-type par catalyst behaviour. Nucl Eng Des 2024;417:112822. https://doi.org/10.1016/j.nucengdes.2023.112822.

[30] Pashchenko D. Comparative analysis of hydrogen/air combustion CFD-modeling for 3D and 2D computational domain of micro-cylindrical combustor. Int J Hydrogen Energy 2017;42(49):29545–56. https://doi.org/10.1016/j.ijhydene.2017.10.070.

[31] Povilaitis M, Jaseliūnaitė J. Simulation of hydrogen-air-diluents mixture combustion in an acceleration tube with flamefoam solver. Energies 2021;14(17):5504. https://doi.org/10.3390/en14175504.

[32] Malakhov AA, Du Toit MH, Avdeenkov AV, Bessarabov DG. Numerical modelling of catalytic hydrogen combustion in passive autocatalytic recombiners: a review. Prog Nucl Energy 2024;171:105199. https://doi.org/10.1016/j.pnucene.2024.105199.

[33] Kim J, Jung J, Kim SH. CFD Modeling for hydrogen removal by a passive autocatalytic recombiner in oxygen-deficient conditions. Nucl Eng Technol 2024:S1738573324002882. https://doi.org/10.1016/j.net.2024.06.028.

[34] Dong Y, Korup O, Gerdts J, Roldán Cuenya B, Horn R. Microtomography-based CFD modeling of a fixed-bed reactor with an open-cell foam monolith and experimental verification by reactor profile measurements. Chem Eng J 2018;353:176–88. https://doi.org/10.1016/j.cej.2018.07.075.

[35] Choi YS, Oh K, Jung K-D, Kim W-I, Koh HL. Regeneration of Pt-Sn/Al_2O_3 catalyst for hydrogen production through propane dehydrogenation using hydrochloric acid. Catalysts 2020;10(8):898. https://doi.org/10.3390/catal10080898.

[36] Barbier J. Reduction of Pt/Al_2O_3 catalysts: effect of hydrogen and of water and hydrochloric acid vapor on the accessibility of platinum. J Catal 1992;137(2):377–84. https://doi:10.1016/0021-9517(92)90165-e.

[37] Du Plessis A, Le Roux SG, Guelpa A. The CT scanner facility at Stellenbosch University: an open access X-ray computed tomography laboratory. Nucl Instrum Methods Phys Res Sect B Beam Interact Mater Atoms 2016;384:42–9. https://doi.org/10.1016/j.nimb.2016.08.005.

[38] Kozhukhova AE, Du Preez SP, Bessarabov DG. Preparation of Pt/Ce–Zr–Y mixed oxide/anodized aluminium oxide catalysts for hydrogen passive autocatalytic recombination. Int J Hydrogen Energy 2022;47(25):12726–38. https://doi.org/10.1016/j.ijhydene.2022.01.246.

[39] Du Preez SP, Jones DR, Bessarabov DG, Falch A, Mota Das Neves Quaresma C, Dunnill CW. Development of a Pt/stainless steel mesh catalyst and its application in catalytic hydrogen combustion. Int J Hydrogen Energy 2019;44(49):27094–106. https://doi.org/10.1016/j.ijhydene.2019.08.168.

[40] Zhang X, Li J, Zhu J, Qiu L. Computational fluid dynamics study on liquefied natural gas dispersion with phase change of water. Int J Heat Mass Tran 2015;91:347–54. https://doi.org/10.1016/j.ijheatmasstransfer.2015.07.117.

[41] Balestrin E, Arruda Guelli Ulson De Souza SM, Valle JAB, Da Silva A. Sensitivity of the turbulent Schmidt number and the turbulence models to simulate catalytic and photocatalytic processes with surface reaction limited by mass transfer. Chem Eng Res Des 2021;170:90–106. https://doi.org/10.1016/j.cherd.2021.03.035.

[42] Rinnemo M, Deutschmann O, Behrendt F, Kasemo B. Experimental and numerical investigation of the catalytic ignition of mixtures of hydrogen and oxygen on platinum. Combust Flame 1997;111(4):312–26. https://doi.org/10.1016/S0010-2180(97)00002-3.

[43] Prabhudharwadkar DM, Aghalayam PA, Iyer KN. Simulation of hydrogen mitigation in catalytic recombiner: Part-I: surface chemistry modelling. Nucl Eng Des 2011;241(5):1746–57. https://doi.org/10.1016/j.nucengdes.2010.09.032.

[44] Tominaga Y, Stathopoulos T. Turbulent Schmidt numbers for CFD analysis with various types of flowfield. Atmos Environ 2007;41(37):8091–9. https://doi.org/10.1016/j.atmosenv.2007.06.054.

[45] Orszulik M, Fic A, Bury T. CFD modeling of passive autocatalytic recombiners. Nukleonika 2015;60(2):347–53. https://doi.org/10.1515/nuka-2015-0050.

[46] Appel C, Mantzaras J, Schaeren R, Bombach R, Kaeppeli B, Inauen A. An experimental and numerical investigation of turbulent catalytically stabilized channel flow combustion of hydrogen/air mixtures over platinum. Proc Combust Inst 2002;29(1):1031–8. https://doi.org/10.1016/S1540-7489(02)80130-4.

[47] Deutschmann O, Schmidt R, Behrendt F, Warnat J. Numerical modeling of catalytic ignition. Symp. Int. Combust. 1996;26(1):1747–54. https://doi.org/10.1016/S0082-0784(96)80400-0.

[48] Deutschmann O, Maier LI, Riedel U, Stroemman AH, Dibble RW. Hydrogen assisted catalytic combustion of methane on platinum. Catal Today 2000;59(1–2):141–50. https://doi.org/10.1016/S0920-5861(00)00279-0.

[49] Twigg MV, Richardson JT. Theory and applications of ceramic foam catalysts. Chem Eng Res Des 2002;80(2):183–9. https://doi.org/10.1205/026387602753501906.

[50] Meille V. Review on methods to deposit catalysts on structured surfaces. Appl Catal Gen 2006;315:1–17. https://doi.org/10.1016/j.apcata.2006.08.031.

[51] Sanap KK, Varma S, Waghmode SB, Bharadwaj SR. Supported Pt nanoparticles for the hydrogen mitigation application. Int J Hydrogen Energy 2014;39(27):15142–55. https://doi.org/10.1016/j.ijhydene.2014.07.087.

[52] Bianchi E, Heidig T, Visconti CG, Groppi G, Freund H, Tronconi E. Heat transfer properties of metal foam supports for structured catalysts: wall heat transfer coefficient. Catal Today 2013;216:121–34. https://doi.org/10.1016/j.cattod.2013.06.019.
[53] Rożeń A. Modelling of a passive autocatalytic hydrogen recombiner – a parametric study. Nukleonika 2015;60(1):161–9. https://doi.org/10.1515/nuka-2015-0002.
[54] Gera B, Verma V, Chattopadhyay J. Development and validation of diffusion based CFD model for modelling of hydrogen and carbon monoxide recombination in passive autocatalytic recombiner. Nucl Eng Technol 2023;55(9):3194–201. https://doi.org/10.1016/j.net.2023.06.005.
[55] Razza S, Heidig T, Bianchi E, Groppi G, Schwieger W, Tronconi E, Freund H. Heat transfer performance of structured catalytic reactors packed with metal foam supports: influence of wall coupling. Catal Today 2016;273:187–95. https://doi.org/10.1016/j.cattod.2016.02.058.
[56] Liu PS. A new method for calculating the specific surface area of porous metal foams. Phil Mag Lett 2010;90(6):447–53. https://doi.org/10.1080/09500831003745571.
[57] Meynet N, Bentaïb A, Giovangigli V. Impact of oxygen starvation on operation and potential gas-phase ignition of passive auto-catalytic recombiners. Combust Flame 2014;161(8):2192–202. https://doi.org/10.1016/j.combustflame.2014.02.001.
[58] Sinn C, Kranz F, Wentrup J, Thöming J, Wehinger GD, Pesch GR. CFD simulations of radiative heat transport in open-cell foam catalytic reactors. Catalysts 2020;10(6):716. https://doi.org/10.3390/catal10060716.